Thermodynamics of Fe-Rich Intermetallics along the Rare Earth Series

D. Gozzi,* M. Iervolino, and A. Latini

Dipartimento di Chimica, Università di Roma *La Sapienza*, Piazzale Aldo Moro, 5 - 00185 Roma, Italy

A set of thermodynamic properties of the Fe-rich part of the Fe/rare earth (RE) systems is presented for almost all the elements in the rare earth series. This set of data comes entirely from electromotive force (emf) vs *T* experimental measurements obtained by galvanic cells with a CaF_2 single crystal as the electrolyte. The standard enthalpy and entropy of formation of RE_2Fe_{17} intermetallics have been obtained and compared with previous results found for the RE_2Ni_{17} intermetallics. The enthalpy of formation of RE_2Fe_{17} intermetallics is decidedly less exothermic than the enthalpy of formation of RE_2Ni_{17} with the exception of the value of Pr_2Fe_{17}, which is endothermic. The RE_2Fe_{17} entropy of formation is always positive contrary to the values of RE_2Ni_{17}. For comparison purposes, the thermodynamic data of Y_2Fe_{17} and Dy_2Co_{17} have also been determined. The RE solubility in Fe has been evaluated by the shift of the bcc Fe(110) plane spacing with respect to pure Fe as shown by corresponding X-ray diffraction (XRD) data. Along the RE series, the atomic fraction of RE in the Fe solid solution changes from $(1.2 \pm 0.1)\cdot10^{-4}$ for Er to $(9.2 \pm 0.2)\cdot10^{-4}$ for Ho. The values of the thermodynamic activity of RE coexisting between the RE_2Fe_{17}-rich phase and the Fe solid solution are reported along the series, and the related partial excess free energy is given as electronic and dilatation contributions. The electronic partial excess free energy of RE_2Fe_{17} intermetallics is practically independent of the dilatation term contrary to the RE_2Ni_{17} intermetallics.

1. Introduction

Since the sixties, intermetallic compounds have drawn great attention for understanding of the chemical bond due to their peculiarity. This made them very interesting for both theoretical approaches and application purposes. Among the large family of intermetallics that can be synthesized and studied, the binary and ternary systems containing rare earth and transition-metal elements were particularly considered. The interaction of d and f orbitals produces relevant properties, and such compounds can be superconductors, good permanent magnets, efficient catalysts and electrocatalysts, and hydrogen storage systems as well as, in some cases, promising structural materials.

A lot of work[1−7] related to their physicochemical properties has been done, particularly phase diagrams, but the whole picture is still incomplete. In fact, notwithstanding such large interest, thermodynamic data concerning heat capacities, formation enthalpies, and entropies are for some systems practically absent in the literature. In general, among the experimental[8−14] works, calorimetric data can be found more frequently, and different techniques such as combustion calorimetry,[10] direct synthesis calorimetry,[8,9,11] and solution calorimetry[12−14] have been used. To derive the thermodynamics, measurements in reversible conditions are needed. To do this, the measurements of vapor pressure[15−17] and electromotive force (emf) of solid-state galvanic cells[18−21] are the most suited techniques. The emf method when applicable is one of the most accurate. Papers published by our group showed the applicability of the method for determining the thermodynamic properties of some aluminides[22] and RE_2Ni_{17} intermetallics[23−25] with the elements of the rare earth series.

The scope of this work was to determine the thermodynamic data of the RE_2Fe_{17} intermetallics that are practically unknown and to compare them with those already obtained for the RE_2Ni_{17} intermetallics.[25] A further objective of the present study is the evaluation of the thermodynamic data of RE_2Me_{17} along the metal transition, Me, series (Fe→Co→Ni) and along the rare earth series (La→Gd→Lu).

2. Experimental Section

The galvanic cell type utilized for all the investigated intermetallics is

$$(-)\ \mathrm{Mo|RE,\ REF_y|CaF_2\ (s.c.)|RE_2Fe_{17},\ Fe_{ss},\ REF_y|Mo}\ (+) \quad (1)$$

where Fe_{ss} is the RE saturated solution of Fe in equilibrium with the RE_2Fe_{17} intermetallic phase produced by the eutectic reaction $L \leftrightarrow RE_2Fe_{17}(s) + Fe_{ss}$. REF_y is the RE fluoride. The electrolyte is a CaF_2 single crystal (s.c.), (111) oriented, shaped as an 8 mm diameter × 2 mm thick disk with polished surfaces. The cell is assembled in a Knudsen cell-like holder (see Figure 1) using the classical sandwich-type arrangement. As reported elsewhere,[23−25] we modified the well-accepted experimental procedure of emf vs *T* measurements by performing them under molecular effusion conditions; therefore, a high vacuum is required. This change is mandatory when the vapor pressure of at least one of the galvanic cell components is high at the operating temperatures. To utilize symmetric galvanic cells as cell 1, pure rare earth elements must be used in the anode. At the operating temperature of the cell, which is in the range from (500 to 900) °C, the vapor pressure of some rare earth elements is relatively high, particularly, for Sm, Eu, and Yb. As discussed elsewhere,[23−25] in the above conditions, the treatment of emf vs *T* data should be changed with respect to the standard treatment of the solid electrolyte galvanic cells if the effusion occurs readily.

Intermetallic Synthesis. The samples were synthesized by melting the mixture of the components, rare earth (purity from

* Corresponding author. Email: daniele.gozzi@uniroma1.it.

10.1021/je7003353 CCC: $37.00
Published on Web 10/11/2007

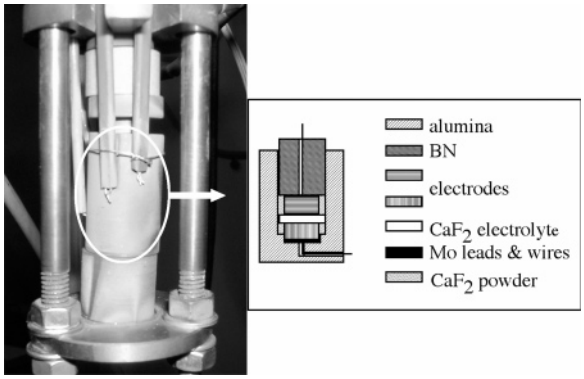

Figure 1. Assembly of galvanic cell 1 inside the latticework is shown. Three S-type thermocouples are positioned close to the cell. Two of them are used to check the isothermal condition of the cell. The third thermocouple is utilized to drive the furnace power control. A scheme of the cell holder is also reported with an effusion hole on the top. This hole is also the way out for the Mo lead.

(99 to 99.999) %) and Fe (99.99 wt % nominal purity), with (91 to 94) atom % Fe. The preparation occurred by melting the components by an e-gun according to the procedure reported elsewhere.[26] The microstructure of the alloys was studied using standard optical and electron metallographic methods. Quantitative electron probe microanalysis was also carried out using an energy dispersive X-ray analyzer (EPMA) to confirm the final composition of the samples. The X-ray analysis was carried out on powder samples using a Bragg−Brentano diffractometer (Panalytical X'Pert Pro).

Table 1 shows some information related to the available phase diagrams of the RE−Fe systems investigated with RE = Pr,[27] Nd,[28] Gd,[29] Tb,[30] Dy,[31] Ho,[32] Er,[33] and Lu.[34] Data concerning the Y−Fe[35] and RE−Co[36] systems that will be considered in the Discussion section are also reported in the same table.

Preparation of Electrodes and Cell Assembling. All the details of the experimental setup are reported in the literature.[23−25] Only the essential information will be reported here.

The emf measurements were carried out in a high-vacuum vertical furnace made of a W(ThO_2) resistor. The inconel spring-loaded latticework (see Figure 1) was utilized for positioning the holder of the electrochemical cell in the isothermal zone of the furnace. The vertical force applied to the cell is maintained at a preset value by a feedback motion device in such a way as to compensate the size changes due to the temperature variations. In this way, the contact pressure at the electrode/electrolyte interface is independent of temperature. The effusion cell is machined from a workable alumina rod (Aremco, USA). It contains the electrodes, electrolytes, and Mo lead wires. Two small holes (1 mm diameter) serve as an outlet for the Mo wires and cell outgassing. All the components of the cell were shaped as small cylinders assembled as a sandwich with the electrolyte in the middle as shown in Figure 1.

The electrodes have been prepared in a glovebox filled with inert and dry atmosphere according to the criterion of establishing the polyphasic coexistence through a close contact among the powder particles. Following the well-established standard procedure, the pure solid phases, as fine powders, have been mixed in acetone and, after evaporation of the solvent, pressed in a stainless steel mold for obtaining cylinders 6 mm in diameter × (3 to 5) mm in height. All the pure rare earth metals and their respective fluorides (99.99 %, 325 mesh), both as powders, were purchased from Smart Elements (Austria) and Sigma-Aldrich (Italy), respectively. The flat surfaces of electrodes were gently polished in such a way as to be in perfect contact with the electrolyte surfaces. The total length of the cells was never greater than 12 mm. The electrical leads were realized by Mo wires up to the feedthroughs of the furnace flange. The temperature was measured by two S-type (Pt/Pt−Rh 10 %) thermocouples. Another S-type thermocouple was used to drive the furnace power control. Before starting the emf measurements, the system was carefully flushed with Ar (O_2 < 1 ppm, H_2O < 1 ppm) and then outgassed by following a standard procedure, which did not allow an increase in the temperature of the cell if the pressure inside the furnace was greater than $5 \cdot 10^{-6}$ mbar. This procedure required at least 2 days. The total pressure during the experiment was maintained below $1 \cdot 10^{-7}$ mbar. The emf measurements were performed by means of a high-impedance preamplifier (10^{15} ohm, typical bias current 40 fA) connected to one of the analogue input channels of a data logger. The total precision in reading the emf was less than 50 μV. A data logger connected to a personal computer read the furnace temperature and pressure as well as the emf. The stability of the temperature of the furnace at the set temperature was always within 1 K. The temperature changes throughout the experiments were performed by programmed ramps with a slope of |2| K·min^{-1}.

3. Data Evaluation Procedure

It can be shown[23,24] that the reaction Gibbs energy, $\Delta_r G$, of cell 1 is given by the equation

$$\Delta_r G = \Delta_r G^\theta = \Delta G^\theta_{cell} - q\beta\Delta_v G^\theta \quad (2)$$

because the activity of RE in the anode is unity. ΔG^θ_{cell} is the standard free energy of the cell reaction, and $\Delta_v G^\theta$ is the standard free energy of RE vaporization. The coefficients q and β are, respectively, equal to

$$q = \sigma_v[1 - (p/p_{eq})] = \sigma_v[1 - \exp(\Delta_v G/RT)] \quad (3)$$

$$\beta = (2 - 19h)/(1 - h) \quad (4)$$

and p and p_{eq} are, respectively, the vapor pressures of RE out of equilibrium and at equilibrium with the condensed phase. σ_v is the vaporization coefficient, which is ≈1 for metals. The β coefficient depends on both the stoichiometry of the cell reaction

$$[(2 - 19h)/(1 - h)]\mathrm{RE(s)} + [17/(1 - h)]\mathrm{RE}_h\mathrm{Fe}_{1-h}\mathrm{(s)} = \mathrm{RE}_2\mathrm{Fe}_{17}\mathrm{(s)} \quad (5)$$

and the solid solubility of RE in Fe represented by h. When $h = 0$, reaction 5 becomes the formation reaction of the RE_2Fe_{17} intermetallic. Throughout the text, the thermodynamic quantities written with subscript r or f refer, respectively, to $h \neq 0$ and $h = 0$. The magnitude of h and its influence on the value of the enthalpy and entropy of formation of the intermetallic compound will be discussed later on. Depending on the value of the ratio p/p_{eq}, q can be practically zero or close to 1 or negative. In practice, because the whole system is under high vacuum, the situation $q < 0$ cannot be achieved at steady state. When $q = 0$ nothing changes with respect to the standard emf measurements of galvanic cells. Due to the very low vapor pressures of the REs studied (at 1000 K, the vapor pressure values[37] range from $3.3 \cdot 10^{-13}$ mbar for Lu to $1.6 \cdot 10^{-6}$ mbar for Dy), the relationship $p_m \approx p \approx p_{eq}$ holds, with p_m being the pressure measured inside the HV furnace. This implies $q = 0$ in all the calculations. If $q = 1$, i.e., when in the presence of a high volatile

Table 1. Intermetallic Phases in the RE−Fe Systems Investigated

RE in RE−Fe system	intermetallic phases RE_xFe_y (x:y)	Fe richest phase reaction	Fe at %	T/°C	ref
Pr[a]	2:17	L→ Pr_2Fe_{17}+Fe_{ss}	89	1375	27
Nd[b]	2:17	L→ Nd_2Fe_{17}+Fe_{ss}	89	1483	28
Gd	1:2_1:3_6:23_2:17	L→ Gd_2Fe_{17}+Fe_{ss}	89	1608	29
Tb	1:2_1:3_6:23_2:17	L→ Tb_2Fe_{17}+Fe_{ss}	89	1585	30
Dy	1:2_1:3_6:23_2:17	L→ Dy_2Fe_{17}+Fe_{ss}	89	1633	31
Ho	1:2_1:3_6:23_2:17	L→ Ho_2Fe_{17}+Fe_{ss}	89	1611	32
Er	1:2_1:3_6:23_2:17	L→ Er_2Fe_{17}+Fe_{ss}	89	1629	33
Lu	1:2_1:3_6:23_2:17	L→ Lu_2Fe_{17}+Fe_{ss}	89	1593	34
Y−Fe	1:2_1:3_6:23_2:17	L→ Y_2Fe_{17}+Fe_{ss}	89	1623	35
Dy−Co	3:1_12:7_4:3_1:2_1:3_2:7_1:5_2:17	L→ Co_2Fe_{17}+Fe_{ss}	89	1663	36

[a] $PrFe_2$ and $PrFe_7$ are also reported in the database of the International Center for Diffraction Data. The former is a metastable phase. [b] Nd_4Fe_6, Nd_5Fe_{17}, and $NdFe_7$ are also reported in the database of the International Center for Diffraction Data. The first two intermetallics are metastable phases.

Table 2. Evaluation of δ_H and δ_S Parameters According to Equation 10 for the RE_wFe_z Intermetallics

RE_wFe_z	T/K	$\bar{T}$/K	$(H_T^\theta - H_{T_r}^\theta)$ / kJ·mol^{-1} at^{-1}	ref	$^a(H_T^\theta - S_{T_r}^\theta)$ / kJ·mol^{-1} at^{-1}	δ_H	$(S_T^\theta - S_{T_r}^\theta)$ / JK^{-1}·mol^{-1} at^{-1}	ref	$^a(S_T^\theta - S_{T_r}^\theta)$ / JK^{-1}·mol^{-1} at^{-1}	δ_S
$GdFe_2$	300	0	5.81	37	6.10	0.95	38.63	37	40.89	0.94
$TbFe_2$	300	0	6.09	37	6.19	0.98	40.60	37	42.56	0.95
$DyFe_2$	300	0	6.21	37	6.03	1.03	41.62	37	43.35	0.96
$HoFe_2$	300	0	6.20	37	5.72	1.08	42.46	37	43.44	0.98
$ErFe_2$	300	0	6.13	37	5.51	1.11	42.28	37	43.01	0.98
$LuFe_2$	300	0	5.33	37	5.16	1.03	35.30	37	35.09	1.01

[a] Data calculated by the Kopp rule through the enthalpy and entropy functions from Ivtanthermo.[37]

RE, the effect of the vaporization on the energy balance of the electrochemical cell should be taken into account. In this case, the cell reaction is

$$\beta(1+q)\mathrm{RE(s)} + \alpha\mathrm{RE}_h\mathrm{Fe}_{1-h}\mathrm{(s)} = \mathrm{RE_2Fe_{17}(s)} + \beta q\mathrm{RE(g)} \quad (6)$$

which becomes reaction 5, through eq 4, when vaporization of the RE is negligible ($q \approx 0$). The coefficient α is equal to $17/(1-h)$. This means that ΔG_{cell}, the free energy change associated with the galvanic cell reaction, embeds the free energy change of RE vaporization. Therefore, it is necessary to subtract the above quantity, as stated by eq 2, to have data corresponding to reaction 5. According to eq 2, the measured emf data are standard emf values E^θ that are related to $\Delta G^\theta_{\mathrm{cell}}$ by the equation $\Delta G^\theta_{\mathrm{cell}} = -y\beta FE^\theta$ where F is the Faraday's constant and y is the number of electrons exchanged in the cell reaction. This quantity is also the RE valence state. The best fitting straight line through n experimental points should obey the equation

$$E^\theta = -\frac{1}{y\beta F}(\Delta_r H^\theta + q\beta\Delta_v H^\theta) + \frac{T}{y\beta F}(\Delta_r S^\theta + q\beta\Delta_v S^\theta) \quad (7)$$

from which $\Delta_r H^\theta_{\bar{T}}$ and $\Delta_r S^\theta_{\bar{T}}$ are obtained at the average temperature $\bar{T} = \sum_i T_i/n$, respectively, from intercept ι and slope σ, as given below

$$\Delta_r H^\theta_{\bar{T}} = -y\beta F\iota - q\beta\Delta_v H^\theta_{\bar{T}} \quad (8)$$

$$\Delta_r S^\theta_{\bar{T}} = y\beta F\sigma - q\beta\Delta_v S^\theta_{\bar{T}} \quad (9)$$

To correct the values of $\Delta_r H^\theta_{\bar{T}}$ and $\Delta_r S^\theta_{\bar{T}}$ to the reference temperature of 298.15 K, the enthalpy function $(H^\theta_{\bar{T}} - H^\theta_{298})$ and entropy function $(S^\theta_{\bar{T}} - S^\theta_{298})$ of RE_2Fe_{17} intermetallics should be known. Unfortunately, no data can be found in the literature. The above functions can be qualitatively obtained by calculating the deviations δ_H and δ_S from the Kopp rule of known enthalpy and entropy functions of intermetallics, RE_wFe_z, which belong to the same RE−Fe system. Therefore, for RE_wFe_z

$$\delta_H = \frac{(H^\theta_T - H^\theta_{T_r})_E}{(H^\theta_T - H^\theta_{T_r})_K}; \quad \delta_S = \frac{(S^\theta_T - S^\theta_{T_r})_E}{(S^\theta_T - S^\theta_{T_r})_K} \quad (10)$$

where the subscripts E and K refer, respectively, to the experimental and Kopp's rule calculated data. T_r is the reference temperature. The enthalpy and entropy functions $(H^\theta_{\bar{T}} - H^\theta_{298})$ and $(S^\theta_{\bar{T}} - S^\theta_{298})$ of a given RE_2Fe_{17} at $\bar{T}$ are given by

$$(H^\theta_{\bar{T}} - H^\theta_{298}) = \delta_H(H^\theta_{\bar{T}} - H^\theta_{298})_K = \delta_H[2(H^\theta_{\bar{T}} - H^\theta_{298})_{\mathrm{RE}} + 17(H^\theta_{\bar{T}} - H^\theta_{298})_{\mathrm{Fe}}]$$

$$(S^\theta_{\bar{T}} - S^\theta_{298}) = \delta_H(H^\theta_{\bar{T}} - H^\theta_{298})_K = \delta_S[2(S^\theta_{\bar{T}} - S^\theta_{298})_{\mathrm{RE}} + 17(S^\theta_{\bar{T}} - S^\theta_{298})_{\mathrm{Fe}}] \quad (11)$$

The enthalpy and entropy changes of reaction 5 at 298.15 K are given by

$$\Delta_r H^\theta_{298} = \Delta_r H^\theta_{\bar{T}} - \sum_i \nu_i(H^\theta_{\bar{T}} - H^\theta_{298})_i = \Delta_r H^\theta_{\bar{T}} - (\delta_H - 1)(H^\theta_{\bar{T}} - H^\theta_{298})_K$$

$$\Delta_r S^\theta_{298} = \Delta_r S^\theta_{\bar{T}} - \sum_i \nu_i(S^\theta_{\bar{T}} - S^\theta_{298})_i = \Delta_r S^\theta_{\bar{T}} - (\delta_S - 1)(S^\theta_{\bar{T}} - S^\theta_{298})_K \quad (12)$$

4. Results

Table 2 gives the values of δ_H and δ_S evaluated according to the above procedure only for $REFe_2$ intermetallics whose data of the enthalpy and entropy functions are available.[38] The above procedure cannot be applied to the Pr−Fe and Nd−Fe systems because such data are missing. The data for the calculations of the $(H^\theta_{\bar{T}} - H^\theta_{298})$ and $(S^\theta_{\bar{T}} - S^\theta_{298})$ terms in the above functions were taken from the Ivtanthermo database.[37]

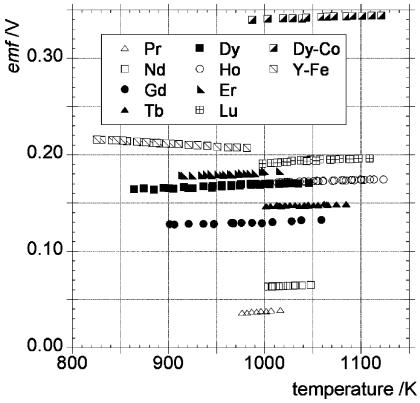

Figure 2. emf vs T curves for all the RE_2Fe_{17} intermetallics examined. The curves obtained for Y_2Fe_{17} and Dy_2Co_{17} are also shown. Note that only Y_2Fe_{17} displays the negative slope.

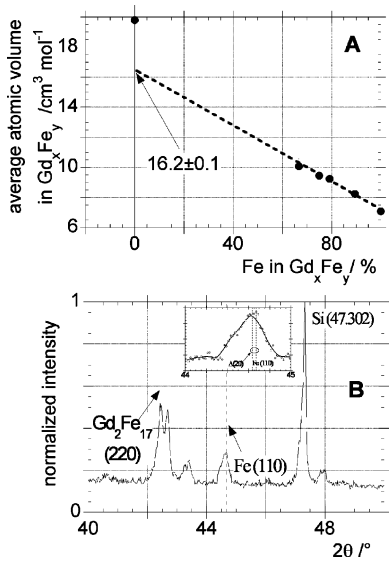

Figure 3. Panel A. Average atomic volume in Gd_xFe_y intermetallics against the atomic fraction of Fe in Gd_xFe_y. The partial atomic volume of Gd at $x_{Gd} \rightarrow 0$ is obtained by linear extrapolation starting from the highest Fe concentrations. Panel B. Evaluation of the 2θ shift (Δ) of the Fe(110) feature due to the solubility of Gd in the Fe solid solution.

Table 3. Coefficients of the Best Fitting Straight Lines through the Experimental *emf vs* T Points. According to Eqs 8 and 9, ι and σ Are, Respectively, the Intercept and Slope

RE in RE_2Fe_{17}	$\bar{T}$ / K	ι / V	$\pm\Delta\iota$ / V	σ / VK^{-1}	$\pm\Delta\sigma$ / VK^{-1}
Pr	995	−0.036	$6\cdot10^{-3}$	$7.4\cdot10^{-5}$	$6\cdot10^{-6}$
Nd	1022	0.021	$2\cdot10^{-3}$	$4.2\cdot10^{-5}$	$2\cdot10^{-6}$
Gd	972	0.101	$3\cdot10^{-3}$	$2.9\cdot10^{-5}$	$3\cdot10^{-6}$
Tb	1041	0.122	$4\cdot10^{-3}$	$2.4\cdot10^{-5}$	$4\cdot10^{-6}$
Dy	965	0.129	$2\cdot10^{-3}$	$4.0\cdot10^{-5}$	$2\cdot10^{-6}$
Ho	1066	0.143	$1\cdot10^{-3}$	$2.8\cdot10^{-5}$	$1\cdot10^{-6}$
Er	959	0.137	$5\cdot10^{-3}$	$4.5\cdot10^{-5}$	$5\cdot10^{-6}$
Lu	1054	0.149	$4\cdot10^{-3}$	$4.7\cdot10^{-5}$	$4\cdot10^{-6}$
Y_2Fe_{17}	895	0.2640	$9\cdot10^{-4}$	$-5.8\cdot10^{-5}$	$1\cdot10^{-6}$
Dy_2Co_{17}	1059	0.307	$3\cdot10^{-3}$	$3.3\cdot10^{-5}$	$3\cdot10^{-6}$

Figure 2 shows the experimental emf vs T data for all the investigated RE_2Fe_{17} intermetallics. The coefficients with associated errors of the best fitting straight lines are reported in Table 3.

For correct calculation of the thermodynamic quantities, it is necessary to know β given by eq 4 through the value of the RE solubility in Fe, named h in the above equation. In a previous work,[25] we evaluated h by measuring the 2θ shift in the XRD

Table 4. Solubility Data of RE in Fe at $x_{RE} \rightarrow 0$ from XRD Spectra and Calculation of Coefficient β[a]

RE in RE_2Fe_{17}	$\bar{V}_{RE}(x_{RE}\rightarrow0)$ / $cm^3\cdot mol^{-1}$	Δ / pm	$\Delta2\theta$ / °	h / %	β
Y	16.9 ± 0.1	0.006	−0.092	0.167 ± 0.001	1.972
Pr	16.7 ± 0.1	0.002	−0.035	0.056 ± 0.002	1.990
Nd	16.5 ± 0.2	0.001	−0.016	0.028 ± 0.001	1.995
Gd	16.2 ± 0.1	0.002	−0.037	0.059 ± 0.002	1.990
Tb	16.0 ± 0.2	0.002	−0.030	0.060 ± 0.001	1.989
Dy	15.8 ± 0.2	0.001	−0.013	0.030 ± 0.003	1.994
Ho	15.6 ± 0.2	0.003	−0.037	0.092 ± 0.002	1.984
Er	15.5 ± 0.1	0.004	−0.073	0.012 ± 0.001	1.998
Lu	15.0 ± 0.3	0.002	−0.033	0.065 ± 0.003	1.989

[a] $\Delta(2\theta) = (2\theta)_{Ni_{ss}} - (2\theta)_{Ni}$; $\Delta(a_{Fe_{ss}} - a_{Fe}) = (\lambda/\sqrt{2})\{[\sin(\chi_{ss}/2)]^{-1} - [\sin(\chi/2)]^{-1}\}$; $\chi[Fe(110)] = (2\theta)_{110} = 44.671°$; $\beta = (2 - 19h)/(1 - h)$; 1 $cm^3\cdot mol^{-1} = 10^{-21}N_A$ $nm^3\cdot at^{-1}$.

Table 5. Crystallographic Data for All the Intermetallics in the Gd−Fe System[a]

Gd_xFe_y	crystalline system	a / pm	b / pm	c / pm	V_u / 10^{-3} nm^3	Z	$\bar{V}_a$ / 10^{-3} nm^3
$GdFe_2$	Fd $\bar{3}$m	738	−	−	401.94	8	16.74
$Gd\ Fe_3$	R $\bar{3}$m	514.8	−	2462	565.06	9	15.70
Gd_6Fe_{23}	Fm $\bar{3}$m	1212	−	−	1780	4	15.34
Gd_2Fe_{17}	$P6_3/mmc$	839	−	853	520	2	13.68

[a] 1 $cm^3\cdot mol^{-1} = 10^{-21}N_A$ $nm^3\cdot at^{-1}$; V_u = volume of the unit cell; Z = number of molecules in the unit cell; $\bar{V}_a = V_u/Z(x + y)$ = average atomic volume.

spectrum of $RE_2Ni_{17} + Ni_{ss}$ samples with respect to the (111) most intense feature of pure Ni. Such a procedure requires calculation of the partial molar volume of RE at infinite dilution, $\bar{V}_{RE}(x_{RE} \rightarrow 0)$, where x_{RE} is the atomic fraction of RE. To do this, the average atomic volume, $\bar{V}_a = V_u/Z(x + y)$, of the atoms in the lattice unit cell of RE_xFe_y is considered as a function of the stoichiometry of all the intermetallics belonging to a given RE−Me system. For length reasons, the procedure will be shown only for the Gd−Fe system, whereas the complete set of results has been summarized in Table 4. Consider Table 5 where the crystallographic parameters of all the intermetallics of the Gd−Fe system are reported. To obtain h, i.e., $x_{RE} \rightarrow 0$, a linear dependency from the atomic fraction of RE, x_{RE}, of the Fe lattice parameter, $a_{Fe_{ss}}$, in the Fe solid solution was assumed according to the equation

$$a_{Fe_{ss}} = a_{Fe} + (\partial a_{Fe}/\partial x_{Fe})x_{RE} \tag{13}$$

This assumption is well justified when $x_{RE} \rightarrow 0$ because the Henry behavior of the solid solution holds.[39,40] The partial atomic volume of RE at $x_{RE} \rightarrow 0$, $\bar{V}_{RE}(x_{RE} \rightarrow 0)$, can be obtained by extrapolation of curves $\bar{V}_a$ vs x_{Fe} at $x_{Fe} \rightarrow 1$. The extrapolated straight line should obey the equation

$$\bar{V}_{RE}(x_{RE} \rightarrow 0) = \frac{1}{2}\left(V^0_{Fe} + \frac{\partial \bar{V}_a}{\partial x_{Fe}}\right) \tag{14}$$

where $V^0_{Fe} = N_A a^3_{Fe}$ is the volume of an Avogadro number, N_A, of lattice unit cells of bcc Fe, each one having two atoms. Combining eqs 13 and 14, h can be calculated by the equation

$$h = 3\Delta/a_{Fe}\left[\frac{2\bar{V}_{RE}(x_{RE} \rightarrow 0)}{V^0_{Fe}} - 1\right] \tag{15}$$

where $\Delta = (a_{Fe_{ss}} - a_{Fe}) = (\lambda/\sqrt{2})\{[\sin(\chi_{ss}/2)]^{-1} - [\sin(\chi/$

Table 6. Enthalpy and Entropy of Reaction $[(2 - 19h)/(1 - h)]RE(s) + [17/(1 - h)]RE_hFe_{1-h}(s) = RE_2Fe_{17}(s)$[e]

RE in RE_2Fe_{17}	$\bar{T}$ / K	$\Delta_r H^\theta_T$ / kJ·(mol at)$^{-1}$	$\Delta_r H^\theta_{298}$ / kJ·(mol at)$^{-1}$	$^a\Delta_f H^\theta_{298}$ / kJ·(mol at)$^{-1}$	$\Delta_r S^\theta_T$ / JK^{-1}·(mol at)$^{-1}$	$\Delta_r S^\theta_{298}$ / JK^{-1}·(mol at)$^{-1}$
Pr	995	1.09 ± 0.02	−	−6.5	2.24 ± 0.01	−
Nd	1022	−0.64 ± 0.01	−	0.3	1.28 ± 0.01	−
Gd	972	−3.03 ± 0.03	(−2.0)	−0.5	0.88 ± 0.01	3.0
Tb	1041	−3.69 ± 0.02	(−3.3)	−1.3	0.73 ± 0.02	2.6
Dy	965	−3.92 ± 0.01	−4.6	−1.3	1.21 ± 0.02	2.7
			−1.9 ± 25 %[d]			
Ho	1066	−4.32 ± 0.02	−6.7	−5.8	0.85 ± 0.01	1.8
Er	959	−4.17 ± 0.04	−6.6	−2.0	1.37 ± 0.01	2.0
Lu	1054	−4.51 ± 0.02	−5.4	−7.3	1.42 ± 0.02	(1.2)
Y_2Fe_{17}	895	−7.93 ± 0.01	−	−8.7	−1.74 ± 0.02	−
	973[b]	−6.38 ± 0.31	−		−1.90 ± 0.28	−
Dy_2Co_{17}	1059	−9.35 ± 0.09	−8.0[c]	−10.4	1.00 ± 0.09	−

[a] Data calculated from Miedema.[2] [b] Ref 42. [c] Ref 43. [d] Ref 14. [e] Data within round brackets should not be considered reliable.

Table 7. $\Delta\bar{G}^e_{RE}$ and $\Delta\bar{G}^d_{RE}$ contributions to the Partial Excess Free Energy of RE, $\Delta\bar{G}^E_{RE}$, Calculated at 1000 K According to Equation 17

RE in RE_2Fe_{17}	h / %	log a_{RE}	$\Delta\bar{G}^E_{RE}$ / kJ·mol^{-1}	$\Delta\bar{G}^d_{RE}$ / kJ·mol^{-1}	$\Delta\bar{G}^e_{RE}$ / kJ·mol^{-1}	RE atomic number
Y	0.167 ± 0.001	−3.58300 ± 0.00008	−14	260	−274	39
Pr	0.056 ± 0.002	−0.5718 ± 0.0005	51	254	−203	59
Nd	0.028 ± 0.001	−0.9457 ± 0.0007	51	248	−197	60
Gd	0.059 ± 0.002	−2.010 ± 0.001	23	238	−215	64
Tb	0.060 ± 0.001	−2.135 ± 0.001	21	232	−211	65
Dy_2Fe_{17}	0.030 ± 0.003	−2.626 ± 0.001	17[a]	226	−209	66
Dy_2Ni_{17}	0.151 ± 0.003	−9.33	−125[b]	172	−297	
Ho	0.092 ± 0.002	−2.4517 ± 0.0009	12	220	−208	67
Er	0.012 ± 0.001	−2.840 ± 0.003	20	217	−197	68
Lu	0.065 ± 0.003	−2.848 ± 0.003	7	201	−194	71

[a] $\gamma_{Dy(Fe)} = 7.73$. [b] $\gamma_{Dy(Ni)} = 2.95\cdot10^{-7}$, ref 25.

Table 8. Enthalpy and Entropy of Reaction $[(2 - 19h)/(1 - h)]Dy(s) + [17/(1 - h)]Dy_hMe_{1-h}(s) = Dy_2Me_{17}(s)$ and Comparison of the Thermodynamic Data along the Fe→Co→Ni Series

Me in Dy_2Me_{17}	$\bar{T}$ / K	$^d\Delta_r H^\theta_{298}$ / kJ·(mol at)$^{-1}$	$\Delta_r H^\theta_T$ / kJ·(mol at)$^{-1}$	$\Delta_r H^\theta_{298}$ / kJ·(mol at)$^{-1}$	$\Delta_r S^\theta_T$ / JK^{-1}·(mol at)$^{-1}$	$\Delta_r S^\theta_{298}$ / JK^{-1}·(mol at)$^{-1}$	$\Delta_r G^\theta_T$ / kJ·(mol at)$^{-1}$	log a_{RE} at $\bar{T}$
Fe[a]	965	−1.3	−3.92 ± 0.06	−4.6	1.21 ± 0.06	2.7	−5.091 ± 0.002	−2.626 ± 0.001
				−1.9[e]				
Co[a,b]	1059	−10.4	−9.35 ± 0.09	−	1.00 ± 0.09	−	−10.419 ± 0.005	−4.882 ± 0.002
Ni[c]	1092	−14.6	−20.3 ± 0.1	−19.1	−1.77 ± 0.09	−2.0 ± 0.1	−18.4 ± 0.2	−9.33 ± 0.09

[a] Present work. [b] $\beta = 2$ was assumed. [c] Ref 25. [d] Calculated data from the Miedema semiempirical model.[2] [e] Ref 14.

$2)]^{-1}\}$ with $\chi = (2\theta)_{110}$ for the most intense XRD line, (110), in the $Gd_2Fe_{17} + Fe_{ss}$ sample and in pure Fe, respectively. λ is the X-ray wavelength of CuKα1 radiation (154.056 pm). Thus, Δ is calculated from the XRD spectrum; $\bar{V}_{RE}(x_{RE}\rightarrow0)$ is obtained from the above-mentioned extrapolation; and $a_{Fe} = 286.65$ pm[41] and h are easily calculated through eq 15.

The average atomic volume in the lattice unit cell, $\bar{V}_a$, as function of Fe content, x_{Fe}, of the intermetallics in the Gd−Fe system is shown in Figure 3A (see also Table 5). By extrapolating the above curve at $x_{Fe}\rightarrow0$, starting from the highest x_{Fe} values, the partial molar volume of Gd in Fe at infinite dilution, $\bar{V}_{Gd}(x_{Gd}\rightarrow0)$, is obtained. A portion of the XRD spectrum of $Gd_2Fe_{17} + Fe_{ss}$ is reported in Figure 3B where the peak of polycrystalline Si, used as an internal reference, is shown together with the peak of Fe in the sample. The latter feature is shifted at lower 2θ values with respect to the line of Fe(110) in pure Fe ($2\theta = 44.671°$)[41] (see inset in Figure 3B). As expected, decreasing 2θ, the lattice parameter increases. This is consistent with the enlargement of the Fe lattice due to the presence of a small quantity of Gd in it. The values of Δ and h are given in Table 4.

Given that β, δ_H, and δ_S are known, it is now possible to compute eqs 9, 10, and 12. The results are reported in Table 6. For comparison purposes, the available literature data for Y_2Fe_{17}[42] and Dy_2Co_{17}[43] are also reported. The correction at 298.15 K of the thermodynamic data obtained at $\bar{T}$ was performed only for the intermetallics having δ_H and δ_S evaluated in Table 2. The correction at 298.15 K should produce more negative values ($\delta_H > 1$) of $\Delta_r H^\theta_{298}$ with respect to $\Delta_r H^\theta_{\bar{T}}$ and more positive values ($\delta_S < 1$) of $\Delta_r S^\theta_{298}$ with respect to $\Delta_r S^\theta_{\bar{T}}$. Therefore, data in Table 6 are reported within round brackets if the above conditions were not satisfied. This implies that the approximation based on the Kopp rule does not work.

5. Discussion

To treat exhaustively the thermodynamic behavior along the rare earth series of the Fe-rich phase in the Fe−RE systems, and for a better comprehension of the text, it is important to divide the whole matter as follows: (i) Calculation of the thermodynamic excess quantities. (ii) Comparison of the data in the Fe→Co→Ni series. (iii) Comparison of the data in the La→Gd→Lu rare earth series.

Calculation of the Thermodynamic Excess Quantities. The Gibbs energy change associated with galvanic cell 1 depends on the chemical potential difference of fluorine, and the positive side of the cell is that where the fluorine chemical potential is higher. Due to the coexistence of RE fluoride with RE at

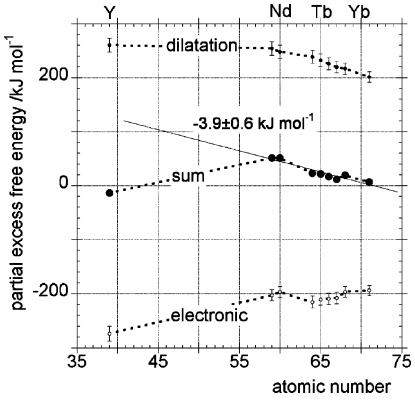

Figure 4. Partial excess free energy, $\Delta\bar{G}^{E}_{RE}$, for all the RE_2Fe_{17} intermetallics investigated is reported. Y_2Fe_{17} is also plotted. The calculation was performed at 1000 K according to eqs 16 to 18. The dilatation and electronic contributions to $\Delta\bar{G}^{E}_{RE}$ are plotted. The error bars were estimated within ± 5 %.

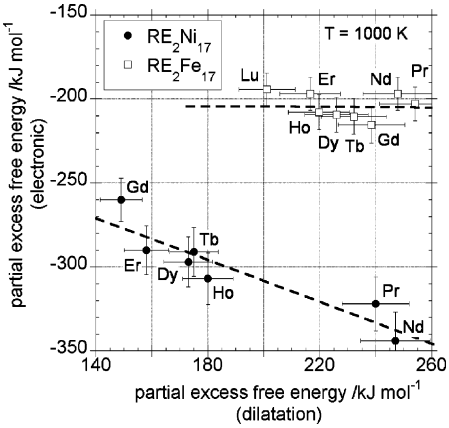

Figure 5. Electronic partial excess free energy is plotted against dilatation partial excess free energy for the RE_2Fe_{17} and RE_2Ni_{17} intermetallics. In the case of RE_2Fe_{17}, the electronic contribution is almost independent of the dilatation contribution to the partial excess free energy.

different activities in both electrodes, the positive side of the cell is also that where the RE activity is lower. This implies that cell 1 behaves as a concentration cell without transport of RE. Therefore, eq 2 can be rewritten as

$$\Delta_r G^\theta = \Delta G^\theta_{cell} - q\beta\Delta_v G^\theta = \beta RT \ln a_{RE} = -\beta y F E^\theta(T) - q\beta\Delta_v G^\theta \quad (16)$$

with $y = 3$ and $a_{RE} = 1$ on the negative side. $E^\theta(T)$ is the experimental linear function of the cell emf vs T, the coefficients being reported in Table 3 for each intermetallic investigated. Through eq 16, the activity value, as a function of temperature, can be calculated as well as the partial excess free energy of RE, $\Delta\bar{G}^{E}_{RE}$, given by

$$\Delta\bar{G}^{E}_{RE} = RT \ln \gamma_{RE} = RT \ln(a_{RE}/h) = \Delta\bar{G}^{e}_{RE} + \Delta\bar{G}^{d}_{RE} \quad (17)$$

where γ_{RE} is the activity coefficient of RE in equilibrium between the phases RE_2Fe_{17} and Fe_{ss}. Elsewhere,[25] as a first approximation, $\Delta\bar{G}^{E}_{RE}$ has been considered as the sum of two excess terms $\Delta\bar{G}^{e}_{RE}$ and $\Delta\bar{G}^{d}_{RE}$. They are, respectively, associated to the electronic contribution due to the transfer of valence electrons from the Fermi level of RE to the Fermi level of Fe and the dilatation of the Fe lattice upon the addition of RE. To reach thermodynamic equilibrium, the electron transfer from RE to Fe occurs because ϕ(Fe) > ϕ(RE),[44] where ϕ is the electron work function. An estimation of $\Delta\bar{G}^{e}_{RE}$ and $\Delta\bar{G}^{d}_{RE}$ can be attempted by using the equation[45] below for evaluating $\Delta\bar{G}^{d}_{RE}$ first

$$\Delta\bar{G}^{d}_{RE}(x_{RE}\rightarrow 0) = (B_{Fe}/b_{Fe})(\bar{V}_{RE} - V^0_{Fe}) + [(B_{Fe}/b_{Fe})V^0_{Fe}/(1 - b_{Fe})][1 - (\bar{V}_{RE}/V^0_{Fe})^{(1-b_{Fe})}] \quad (18)$$

where V^0_{Fe}, B_{Fe}, and b_{Fe} are for Fe at 300 K, respectively, the molar volume (7.05 $cm^3 \cdot mol^{-1}$), bulk modulus at 1 bar ($1.67 \cdot 10^{11}$ $N \cdot m^{-2}$),[46] and the pressure coefficient of B_{Fe}, $(\partial B_{Fe}/\partial p)_T$, (5.29).[46] By taking into account the data reported in Tables 4 and 6 as well as the equations 16 to 18, Table 7 was generated with the excess quantities calculated at 1000 K. The trend of the excess quantities along the rare earth period is also given in Figure 4. There is a regular and almost linear trend of $\Delta\bar{G}^{E}_{RE}$ vs atomic number that means, according to eq 17, an almost exponentially decreasing trend of the RE activity coefficient along the rare earth series. By fitting the $\Delta\bar{G}^{E}_{RE}$ data, one deduces that this quantity decreases constantly by (−3.9 ± 0.6) $kJ \cdot mol^{-1}$ passing from one RE element to the next. In the case of the RE_2Ni_{17} intermetallics, a more negative value [(−4.8 ± 0.4) $kJ \cdot mol^{-1}$] was found.[25] It is worth noticing that, as expected, Y is out of the above trend as shown in Figure 4.

Comparison of the Data in the Fe→Co→Ni Series. By inspection of Table 8, the trend regularity from Fe to Ni of the thermodynamic data of reaction 5, for the formation of Dy_2Me_{17}, appears clearly. The related free energy changes indicate an increasing stability with Dy_2Ni_{17}, about three times more stable than Dy_2Fe_{17}. This behavior was already[12] observed in the systems Gd−Me where the trend $\Delta_f H^\theta$(Ni) < $\Delta_f H^\theta$(Co) < $\Delta_f H^\theta$(Fe) holds. The explanation of this sequence stands in the gradual change of the number of d electrons in Me, the atomic energy level, and the d bandwidth. Colinet[12] et al. attributed the d bandwidth as the predominant effect because the first two cancel. If the Brewer−Engel[47,48] rule was considered, the same sequence would be obtained. In fact, it states that the stability of a RE−Me intermetallic compound increases as the Me d band becomes filled with the s band electrons of RE ($Dy[Xe]6s^2 4f^{10}$). The complete filled d band is obtained only with Ni ($[Ar] 4s^2 3d^8$). The partial excess free energy of Dy in Fe and in Ni[25] is compared in Table 7. The respective values of the activity coefficient are (7.73 and 2.95)·10^{-7}. Therefore, two very different levels of interaction between Dy and transition metal Me exist. This should be attributed[12] to magnetic effects due to Fe and Co. On the other hand, it appears from Table 7 that in Dy_2Fe_{17} the dilatation and electronic contributions are almost balanced, different from the situation in Dy_2Ni_{17}. Furthermore, all the above considerations match with the values of the entropy changes that are positive only in the presence of large magnetic effects as in the case of Dy_2Fe_{17} and Dy_2Co_{17}.

Comparison of the Data in the La→Gd→Lu Rare Earth Series. The dilatation contribution to the partial excess free energy, $\Delta\bar{G}^{d}_{RE}$, is plotted in Figure 5 against the electronic contribution, $\Delta\bar{G}^{e}_{RE}$, for both the RE_2Ni_{17}[25] and RE_2Fe_{17} intermetallics investigated. The uncertainties in the above quantities were evaluated within ± 5 %. Some points arise from inspection of this figure: (i) The electronic term of the RE_2Fe_{17} intermetallics is practically independent of the corresponding dilatation term. In RE_2Ni_{17}, the $\Delta\bar{G}^{e}_{RE}$ term becomes even more negative as the $\Delta\bar{G}^{d}_{RE}$ term increases. (ii) The $\Delta\bar{G}^{e}_{RE}$ values of the RE_2Fe_{17} intermetallics are significantly less negative than the values of the corresponding RE_2Ni_{17}. (iii) The light rare earths, Pr and Nd, show the highest and comparable $\Delta\bar{G}^{d}_{RE}$ values in both systems. It is worth noticing that the crystal structure of these

Table 9. Comparison of the Thermodynamic Data along the Rare Earth Series

RE_2Me_{17}		$\bar{T}$ / K	$\Delta_f H_T^\theta$ / kJ·(mol at)$^{-1}$	$^a\Delta_f H_{298}^\theta$ / kJ·(mol at)$^{-1}$	$\Delta_f S_T^\theta$ / JK^{-1}·(mol at)$^{-1}$	$\Delta_f G_T^\theta$ / kJ·(mol at)$^{-1}$	log a_{RE} at $\bar{T}$	ref
Pr	Fe	995	1.09 ± 0.02	−6.5	2.24 ± 0.01	−1.141 ± 0.001	−0.5718 ± 0.0005	pw
	Ni[b]	955	−17.58 ± 0.02	−13.9	−1.27 ± 0.02	−16.37 ± 0.04	−8.52 ± 0.02	25
Nd	Fe	1022	−0.64 ± 0.01	0.3	1.28 ± 0.01	−1.943 ± 0.001	−0.9457 ± 0.0007	pw
	Ni	998	−18.35 ± 0.01	−13.8	−1.63 ± 0.01	−16.72 ± 0.02	−8.35 ± 0.01	25
Gd	Fe	972	−3.03 ± 0.03	−0.5	0.88 ± 0.01	−3.916 ± 0.001	−2.010 ± 0.001	pw
	Ni	1023	−23.0	−14.3	−5.4	−17.5	−8.56	38
Tb	Fe	1041	−3.69 ± 0.02	−1.3	0.73 ± 0.02	−4.454 ± 0.005	−2.135 ± 0.001	pw
	Ni	1023	−19.03 ± 0.06	−14.8	−1.22 ± 0.02	−17.78 ± 0.08	−8.72 ± 0.04	24
Dy	Fe	965	−3.92 ± 0.01[c]	−1.3	1.21 ± 0.02	−5.091 ± 0.002	−2.626 ± 0.001	pw
	Co	1059	−9.35 ± 0.09	−10.4	1.00 ± 0.09	−10.419 ± 0.005	−4.882 ± 0.002	pw
	Ni	1092	−20.3 ± 0.1	−14.6	−1.77 ± 0.09	−18.4 ± 0.2	−9.33 ± 0.09	23
Ho	Fe	1066	−4.32 ± 0.02	−5.8	0.85 ± 0.01	−5.224 ± 0.001	−2.4517 ± 0.0009	pw
	Ni	1085	−20.37 ± 0.09	−14.1	−1.80 ± 0.09	−18.4 ± 0.2	−8.54 ± 0.09	24
Er	Fe	959	−4.17 ± 0.04	−2.0	1.37 ± 0.01	−5.484 ± 0.006	−2.840 ± 0.003	pw
	Ni	995	−19.7 ± 0.1	−15.0	−1.4 ± 0.1	−18.3 ± 0.2	−9.4 ± 0.1	25
Lu	Fe	1054	−4.51 ± 0.02	−7.3	1.42 ± 0.02	−6.016 ± 0.007	−2.848 ± 0.003	pw
	Ni	−	−	−19.9	−	−	−	−
Y	Fe	895	−7.93 ± 0.01	−8.7	−1.74 ± 0.02	−6.372 ± 0.002	−3.583 ± 0.001	pw
		973	−6.38 ± 0.31		−1.90 ± 0.28	−4.6 ± 0.6	−2.4 ± 0.3	42
	Ni	−	−	−22.2	−	−	−	−

[a] Calculated data from the Miedema semiempirical model.[2] [b] $[(2-15h)/(1-h)]Pr(s) + [13/(1-h)]Pr_hNi_{1-h}(s) = Pr_2Ni_{13}(s)$; pw= present work. [c] From ref 14, $\Delta_f H_{298}^\theta = -1.9$ (± 25 %).

light intermetallics is rhombohedral, whereas the structure of the other ones in the series is hexagonal. (iv) According to eq 17 and Table 7, the balance between $\Delta\bar{G}_{RE}^d$ and $\Delta\bar{G}_{RE}^e$, i.e., $\Delta\bar{G}_{RE}^E$, is always negative for RE_2Ni_{17} and always positive for RE_2Fe_{17} intermetallics. This implies a weak interaction of RE in Fe with respect to the stronger interaction between RE and Ni.

The trend in the thermodynamic data of the RE_2Fe_{17} intermetallics along the RE series is clearly indicated in Table 6. Because the average experimental temperatures are not so different, we can examine the trend of $\Delta_r H_{\bar{T}}^\theta$ instead of the $\Delta_r H_{298}^\theta$ values, which are in some cases missing and affected by the uncertainties connected to the evaluation of the enthalpy function ($H_T^\theta - H_{298}^\theta$). Going from Pr to Lu, the values are even more exothermic starting from $\Delta_r H_{\bar{T}}^\theta$ of Pr, which is endothermic. This kind of evidence was already described in the literature,[14] and it was attributed to the increase of the atomic energy level of the rare earth element. In particular, one can observe that the most relevant changes are related to Pr and Nd, whereas from Gd to Lu the $\Delta_r H_{\bar{T}}^\theta$ values are almost similar. As stated by the authors,[14] the value of $\Delta_f H_{298}^\theta$ of Dy_2Fe_{17} (see Table 6) should be considered with caution due to some experimental uncertainties in the aluminum solution calorimetry, which produce large errors when the heat of formation is low as in the case of Dy_2Fe_{17}. For comparison purposes, an almost complete summary of the thermodynamic data of RE_2Ni_{17} and RE_2Fe_{17}[25] is presented in Table 9. In the same table, the $\Delta_r H_{298}^\theta$ values calculated according the semiempirical model of Miedema[2] are also reported. As stated by the author, those values should be considered to be affected by a systematic uncertainty of more than 10 kJ·mol^{-1}, i.e., for RE_2Me_{17}, > 0.5 kJ (mol·at)$^{-1}$. By inspection of Table 9, at least four key points can be considered:

(a) The enthalpy of formation, $\Delta_f H_{\bar{T}}^\theta$. The inequality $\Delta_f H_{\bar{T}}^\theta(RE_2Ni_{17}) < \Delta_f H_{\bar{T}}^\theta(RE_2Fe_{17})$ is satisfied everywhere. The values are always exothermic with the exception of Pr_2Fe_{17}.

(b) The entropy of formation, $\Delta_f S_{\bar{T}}^\theta$. The inequality $\Delta_f S_{\bar{T}}^\theta(RE_2Ni_{17}) < \Delta_f S_{\bar{T}}^\theta(RE_2Fe_{17})$ is satisfied everywhere. The values related to RE_2Fe_{17} are always positive. According to Germano et al.,[38] the entropy of an intermetallic RE_wMe_z could be written as $S_T^\theta = S_T^\theta(L) + S_T^\theta(E) + wS_T^\theta(m,RE) + zS_T^\theta(m,Me)$ where L and E are, respectively, the lattice and electronic contributions, and $S_T^\theta(m,RE)$ and $S_T^\theta(m,Me)$ are the respective magnetic contributions from the rare earth and Me (Fe, Co, and Ni) atoms to the entropy. Assuming the contribution of some magnetic couplings of RE and Me in the compound is negligible, its entropy of formation is given by $\Delta_f S_T^\theta \approx \Delta S_T^\theta(L) + \Delta S_T^\theta(E)$. If we compare RE_2Me_{17} intermetallics with the same structure, rhombohedral or hexagonal, but with different Me, we have to attribute such large value differences between the $\Delta_f S_T^\theta$ mainly to the electronic term, $\Delta S_T^\theta(E)$. Looking at the electronic structure of Fe ($[Ar]4s^23d^6$) and Ni ($[Ar]4s^23d^8$), it appears evident that the saturation of the d band of the transition metal with the s band electrons of the RE element, as occurs in RE_2Ni_{17} intermetallics, brings it to a lower number of electronic microstates; therefore, $\Delta_f S_T^\theta(RE_2Fe_{17}) > 0$ and $\Delta_f S_T^\theta(RE_2Ni_{17}) < 0$. The progressive filling of the d band of the transition metal is also consistent with the trend of $\Delta_f S_T^\theta$ observed in Dy_2Me_{17} with Me = Fe, Co, Ni. This phenomenon produces effects also on $\Delta_f H_{\bar{T}}^\theta$ which becomes even more exothermic, and the thermodynamic stability (see the column headed $\Delta_f G_{\bar{T}}^\theta$) increases mainly for the enthalpy contribution.

(c) The activity of RE coexisting with RE_2Me_{17} and Me_{ss}. $a_{RE}(Ni) \ll a_{RE}(Fe)$, and the respective values differ by several orders of magnitude. Also in this case, there is a trend along the RE series with $a_{RE}(Me)$ decreasing from Pr to Lu, though this trend is more evident when Me = Fe. In fact, $a_{Pr}(Fe)/a_{Er}(Fe) = 186$, whereas $a_{Pr}(Ni)/a_{Er}(Ni) = 7.6$. So, high activity values of RE in the RE_2Fe_{17} series indicate a very weak interaction between atoms.

(d) The behavior of Y_2Fe_{17}. We studied this system for two reasons: (1) To check our emf technique with the same experimental technique utilized years before on the same Y−Fe system.[42] If the different experimental temperatures of both the measurements on Y_2Fe_{17} (present work and ref 42, see bottom rows of Table 9) are considered, the data found are in good agreement. This supports the present results and the comparison with previous results on RE_2Ni_{17} intermetallics. (2) To compare its thermodynamic properties with Lu_2Fe_{17}. This comparison is very interesting because Lu and Y have a similar outer electronic

configuration (Y ≡ [Kr]$5s^2 4d^1$; Lu ≡ [Xe]$6s^2 4f^{14} 5d^1$) and both the intermetallics have a hexagonal structure. By considering a suitable scaling of $\Delta_f H_T^\theta$ for the different experimental temperatures, it is reasonable to assume that at the lowest temperature, i.e., 895 K, the $\Delta_f H_T^\theta$ values should converge approximately to a similar value, whereas the same reasoning cannot be applied to the $\Delta_f S_T^\theta$ values that are opposite in sign. At first glance, this cannot be attributed either to magnetic contributions, because Y and Lu have practically the same magnetic susceptibility [($187.7 \cdot 10^{-6}$ and $182.9 \cdot 10^{-6}$) $cm^3 \cdot mol^{-1}$, respectively], or to a significant difference of the electron work function values [(3.1 and 3.3) eV, respectively]. At the present time, no reasonable explanation can be supplied. Further investigations are required to look inside this apparent anomaly.

6. Conclusions

According to the scope of this work, the missing thermodynamic data of several RE_2Fe_{17} intermetallics in the RE series have been measured, and they have been compared with previous data obtained for RE_2Ni_{17} intermetallics. The comparison shows an internal consistency and regularity that is expected on the basis of different electronic and magnetic properties of Fe and Ni. This is particularly evident both in the Fe−Co−Ni series, as shown for Dy_2Me_{17} intermetallics, and along the RE series. From the point of view of thermodynamic stability, the RE_2Fe_{17} intermetallics are decidedly less stable than the corresponding intermetallics with Ni. The absence of strong interactions is clearly shown by the high activity values of RE in the Fe solid solution if compared with the corresponding values found in RE_2Ni_{17}.

The whole picture allows confidence in the thermodynamic reliability of the experimental procedure adopted.

Acknowledgment

The planning and development of the studies presented here form a part of an Italian National Research Project entitled “Leghe e Composti Intermetallici: stabilità termodinamica, proprietà fisiche e reattività”.

Literature Cited

(1) Brewer, L. *Systematics of the Properties of the Lanthanides in NATO ASI Ser. C: Mathematical and physical Sciences, No. 109*; Sinha, S. P., Ed.; D. Reidel: Boston, 1983; pp 17−69.
(2) De Boer, F. R.; Boom, R.; Mattens, W. C. M.; Miedema, A. R. *Cohesion in Metals, Transition Metal Alloys*; North Holland: Amsterdam, 1988.
(3) Colinet, C.; Pasturel, A. In *Handbook on the Physics and Chemistry of Rare Earths*; Gschneidner, K. A., Jr., Eyring, L., Eds.; North Holland: Amsterdam, 1994; Vol. 19.
(4) Gschneidner, K. A., Jr. Systematics in lanthanide and actinide solids. *J. Alloys Compd.* **1995**, *223*, 165−169.
(5) Colinet, C. The thermodynamic properties of rare earth metallic systems. *J. Alloys Compd.* **1995**, *225*, 409−422.
(6) Ferro, R.; Borzone, G.; Cacciamani, G.; Parodi, N. Thermodynamics of rare earth alloys systematics and experimental. *Thermochim. Acta* **1998**, *314*, 183−204.
(7) Brewer, L. Prediction of properties of intermetallics using a chemical bonding model. *Metall. Mater. Trans. B* **2000**, *31B*, 603−607.
(8) Jung, W. G.; Kleppa, O. J.; Topor, L. Standard molar enthalpies of formation of palladium aluminide (PdAl), platinum aluminide (PtAl), scandium aluminide ($ScAl_{1.78}$), yttrium aluminide (YAl_2) and lanthanum aluminide ($LaAl_2$). *J. Alloys Compd.* **1991**, *176*, 309−318.
(9) Meschel, V. S.; Kleppa, O. J. Standard enthalpies of formation of 4d aluminides by direct synthesis calorimetry. *J. Alloys Compd.* **1993**, *191*, 111−116.
(10) Snyder, R. L., Thesis, Iowa State University, 1960.
(11) Saccone, A.; Cacciamani, G.; Macciò, D.; Borzone, G.; Ferro, R. Contribution to the study of the alloys and intermetallic compounds of aluminum with the rare-earth metals. *Intermetallics* **1998**, *6*, 201−215.
(12) Colinet, C.; Pasturel, A.; Buschow, K. H. J. Study of the enthalpies of formation in the Gd-(Fe, Co, Pd, Pt) systems. *Metall. Trans. A* **1987**, *18A*, 903−907.
(13) Timofeev, V. S.; Turchanin, A. A.; Zubkov, A. A.; Tomilin, L. A. Enthalpies of formation for the Al-Y and Al-Y-Ni intermetallic compounds. *Thermochim. Acta* **1997**, *299*, 37−41.
(14) Norgren, S.; Hodaj, F.; Azay, P.; Colinet, C. Experimental investigation on the enthalpies of formation of the $DyFe_2$, $DyFe_3$, Dy_2Fe_{17}, $ErFe_2$, $ErFe_3$ intermetallic compounds. *Metall. Mater. Trans. A* **1998**, *29A*, 1367−1374.
(15) Balducci, G.; Brutti, S.; Ciccioli, A.; Gigli, G.; Palenzona, A.; Pani, M. Energetics and Thermodynamic Stability of the Mixed Valence Ytterbium Germanides. *J. Phys. Chem. B* **2007**, *111*, 5132−5139.
(16) Balducci, G.; Ciccioli, A.; Gigli, G.; Gozzi, D.; Anselmi-Tamburini, U. Thermodynamic study of intermetallic phases in the Hf-Al system. *J. Alloys Compd.* **1995**, *220*, 117−121.
(17) Balducci, G.; Brutti, S.; Ciccioli, A.; Gigli, G.; Palenzona, A.; Pani, M. Energetics and Thermodynamic Stability of the Mixed Valence Ytterbium Germanides. *J. Phys. Chem. B* **2007**, *111*, 5132−39.
(18) Kubaschewski, O.; Alcock, C. B. *Metallurgical Thermochemistry*, 5th ed., International Series on Materials Science and Technology; Raynor, G. V., Ed.; Pergamon Press Ltd.: New York, 1979; Chapter 2, Vol. 24.
(19) Rickert, H. *Electrochemistry of Solids*; Springer-Verlag: Berlin, 1982; Chapter 8.
(20) Katayama, I.; Tanigawa, S.; Yamashita, H. Thermodynamic properties of alloys and compounds containing rare earth elements at high temperatures -XIII-. *Kidorui* **2006**, *49*, 9−29.
(21) Katayama, I.; Suzuki, Y.; Yamamoto, Y.; Oishi, T. Activity measurements of solid Ni−In alloys by EMF method with zirconia solid electrolyte. *Monatsh. Chem.* **2005**, *136*, 1955−1.
(22) Borzone, G.; Ciccioli, A.; Cignini, P. L.; Ferrini, M.; Gozzi, D. Thermodynamics of the YAl-YAl_2 system. *Intermetallics* **2000**, *8*, 203−212.
(23) Di Pascasio, F.; Gozzi, D.; Parodi, N.; Borzone, G. Thermodynamic Properties of Me_2Ni_{17} (Me = Sm, Dy, and Yb) Intermetallics by Solid Electrolyte Cells under Effusion Conditions. *J. Phys. Chem. B* **2002**, *106*, 4284−4293.
(24) Cignini, P. L.; Gozzi, D.; Iervolino, M.; Latini, A. Thermodynamics of intermetallics through emf measurements under effusion conditions. *Intermetallics* **2003**, *11*, 1167−1174.
(25) Gozzi, D.; Iervolino, M. Thermodynamics of Ni richest intermetallics along the rare earth series. *Intermetallics* **2005**, *13*, 1172−1183.
(26) Latini, A.; Di Pascasio, F.; Gozzi, D. A new synthesis route to light lanthanide borides: borothermic reduction of oxides enhanced by electron beam bombardment. *J. Alloys Compd.* **2002**, *346*, 311−313.
(27) Ray, A. E. The crystal structure of CeFe7, PrFe7, NdFe7, and SmFe7. *Acta Crystallogr.* **1966**, *21*, 426−430.
(28) Schneider, G.; Henig, E. T.; Petzow, G.; Stadelmaier, H. H. Metastable solidification of iron-rich iron-neodymium-boron alloys. *Z. Metallkd.* **1987**, *78*, 818−820.
(29) Copeland, M. I.; Krug, M.; Armantrout, C. E.; Kate, H. *Iron-gadolinium phase diagram*; No. 5925; Bureau of Mines Report of Investigations, 1962; 15 pp.
(30) Dariel, M. P.; Holthuis, J. T.; Pickus, M. R. The terbium-iron phase diagram. *J. Less Common Met.* **1976**, *45*, 91−101.
(31) Van der Goot, A. S.; Buschow, K. H. J. Dysprosium-iron system: structural and magnetic properties of dysprosium-iron compounds. *J. Less Common Met.* **1970**, *21*, 151−157.
(32) Roe, G. J.; O'Keefe, T. J. Iron-holmium binary system. *Metall. Trans.* **1970**, *1*, 2565−2568.
(33) Buschow, K. H. J.; Van der Goot, A. S. Phase relations, crystal structures, and magnetic properties of erbium-iron compounds. *Phys. Status Solidi* **1969**, *35*, 515−522.
(34) Kolesnichenko, V. F.; Terekhova, V. F.; Savitskii, E. M. Phase diagrams of thulium-iron and lutetium-iron alloys. *Metalloved. Tsvetn. Met. Splavov Nauka* **1972**, *31*, 3.
(35) Du Z.; Zhang, W.; Zhuang, Y. Thermodynamic assessment of the Fe-Y system. *Rare Metals (Beijing)* **1997**, *16*, 52−58.
(36) Buschow, K. H. J. Rare-earth-cobalt intermetallic compounds. *Philips Res. Rep.* **1971**, *26*, 49−64.
(37) *IVTANTHERMO for Windows*, v.3.0; database of thermodynamic properties of individual substances and thermodynamic modeling software; Glushko Thermocenter of RAS: 2005.
(38) Germano, D. J.; Butera, R. A.; Gschneidner, K. A., Jr. Heat Capacity and Thermodynamic Functions of the RFe_2 Compounds (R=Gd, Tb, Dy, Ho, Er, Tm, Lu) over the Temperature Region 8 to 300 K *J. Solid State Chem.* **1981**, *37*, 383−389.
(39) Dischinger, J.; Schaller, H. J. On the constitution and thermodynamics of Ni-Gd alloys *Ber. Bunsenges. Phys. Chem.* **1998**, *102*, 1167−1172.
(40) Rong, Q.; Schaller, H. J. On the constitution and thermodynamics of Ni-Tb alloys. *J. Alloys Compd.* **2004**, *365*, 188−196.

(41) International Center for Diffraction Data, data base JCPDS CARD = 06−0696.
(42) Subramanian, P. R.; Smith, J. F. Thermodynamics of Y-Fe Alloys. *CALPHAD* **1984**, *8*, 295−305.
(43) Schott, J.; Sommer, F. J. Determination of the enthalpies of formation of intermetallic compounds of cobalt and nickel with dysprosium, erbium, and gadolinium. *J. Less Common Met.* **1986**, *119*, 307−317.
(44) Michaelson, H. B. The work function of the elements and its periodicity. *J. Appl. Phys.* **1977**, *48*, 4729−4733.
(45) Schaller, H. J. Electronic and elastic influences on the energetics of alloy formation. *Ber. Bunsenges. Phys. Chem.* **1983**, *87*, 734−741.
(46) Mimkes, J.; Lübbers, M.; Thomas, H. H. Thermophysical properties of cubic elements. *Thermochim. Acta*. **1994**, *245*, 1−19.
(47) Engel, N. Properties of metallic phases as a function of number and kind of bonding electrons. *Powder Met. Bull.* **1954**, *7*, 8−18.
(48) Brewer, L. *Thermodynamic Stability and Bond Character in Relation to Electronic Structure and Crystal Structure in Electronic Structure and Alloy Chemistry of Transition Elements*; Beck, P. A., Ed.; Interscience Publishers, John Wiley: New York, 1963; pp 221−235.

Received for review June 12, 2007. Accepted August 25, 2007. The authors would like to thank the Ministero per la Ricerca Scientifica e Tecnologica (Programmi di rilevante interesse tecnologico) for the financial support.

JE7003353